Optical Materials 147 (2024) 114620

Contents lists available at ScienceDirect

Optical Materials

journal homepage: www.elsevier.com/locate/optmat

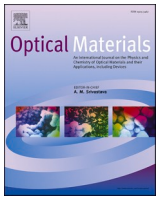

Research Article

Two noncentrosymmetric alkali metal phosphates $MZnPO_4$ (M = Rb, Cs) with honeycomb-like structures

Qun Jing [a,*], Menglin Zhu [a], Lu Li [a], Xu Ji [a], Haiming Duan [a,**], Henglei Chen [a], Ming-Hsien Lee [b]

[a] Xinjiang Key Laboratory of Solid State Physics and Devices, School of Physical Science and Technology, Xinjiang University, 777 Huarui Road, Urumqi, 830017, China
[b] Department of Physics, Tamkang University, New Taipei City, 25137, China

ARTICLE INFO

Keywords:
Nonlinear optical material
Phosphate
Second harmonic generation

ABSTRACT

In recent years, phosphates have become a research hotspot to explore new ultraviolet (UV) nonlinear optical (NLO) materials. Herein, two NLO materials $MZnPO_4$ (M = Rb, Cs) are synthesized by cation substitution in alkali-zinc orthophosphates. Although they crystallize in different space groups $P2_1$ and *Imm*2, respectively, they both have a honeycomb-like topological structure consisting of corner-shared PO_4 and ZnO_4 tetrahedra and separated by "M" cations. Two compounds exhibit mild powder second harmonic generation (SHG) responses (1.2 and 0.5 × KDP for $RbZnPO_4$ and $CsZnPO_4$, respectively) with type I phase matching behaviors and short absorption edges (226 nm for $RbZnPO_4$ and 231 nm for $CsZnPO_4$). Furthermore, their thermal properties, infrared (IR) spectra and theoretical calculations are also mentioned in the paper. The synthesis and structure-property relationship described in the system will enable discovery of new NLO materials.

1. Introduction

Nonlinear optical (NLO) crystals can realize laser frequency conversion, expand spectral wavelength, and modulate beam intensity and phase, so they are the critical materials in the field of optoelectronics, especially in progressive laser science and technology [1–4]. Since the discovery of $Ba_3P_3O_{10}X$ (X = Cl, Br) [5], the phosphates have become a new system for exploring deep-ultraviolet (DUV) NLO materials. Phosphates usually have the following four advantages, including (i) P–O tetrahedral groups have no obvious absorption in the ultraviolet region, which is conducive to the light wave passing through the ultraviolet and even deep ultraviolet region, (ii) the structure of phosphate is usually rigid, which is conducive to improving its chemical stability and thermal stability, (iii) P–O groups have a rich structure, which is conducive to the exploration of new compounds, (iv) phosphates are environmentally friendly and easy to grow crystals. So far, a lot of phosphates, for example, $LiCs_2PO_4$ [6], $LiHgPO_4$ [7], $Ba_2NaClP_2O_7$ [8], β-$Cd(PO_3)_2$ [9], $(NH_4)_2PO_3F$ [10], $(NH_4)_3(H_3O)Zn_4(PO_4)_4$ [11], were reported as promising NLO materials. However, weak second-order NLO susceptibility and small birefringence of phosphates are always the weaknesses to overcome. To improve the second harmonic generation (SHG) response of phosphates, the strategy of introducing NLO-active basic building unit (BBU) is usually chosen [12,13]. The Zn^{2+} cation, as a d^{10} transition metal, has 18e electron configuration with strong polarizability and significant deformability and can eliminate unwanted absorption edge red shifting. Guided by this idea, a number of NLO materials were discovered, such as $CaZn_2(BO_3)_2$ (3.8 × KDP, <190 nm) [14], $Ba_3(ZnB_5O_{10})PO_4$ (4 × KDP, 180 nm) [15], $Cs_3Zn_6B_9O_{21}$ (3.3 × KDP, <200 nm) [16] and $AZn_2BO_3X_2$ (A = K, Rb, NH_4; X = Cl, Br) (2.53–3.01 × KDP, 190–214 nm) [17].

Single-site substitution method is a common and simple method for synthesizing compounds, in which one cation or anion in the parent structure is replaced by another ion in the same family of the periodic table. Once one of the ions is replaced, stoichiometric similar compounds probably exhibit different properties due to different ion sizes [18]. There are many successful examples such as $ABe_2BO_3F_2$ (A = NH_4, Na, K, Rb, Cs) [19–22], AB_4O_6F (A = NH_4, Na, K, Rb, Cs) [23–27], $ABCO_3F$ (A = K, Rb, Cs; B═Ca, Sr, Ba) [28,29], $M_4Mg_4(P_2O_7)_3$ (M = K, Rb) [30], $A_3BBi(P_2O_7)_2$ (A = K, Rb, Cs; B═Sr, Ba, Pb) [31–33], etc. In this paper, we successfully synthesized $RbZnPO_4$ and $CsZnPO_4$ by single-site substitution method based on $AZnPO_4$ (A = Li, K) [34]. The crystal structures of $CsZnPO_4$ (*Imm*2, No.44) is reported first, and $RbZnPO_4$ ($P2_1$, No.4) was reported by Elammari [35], their NLO optical properties were not studied. In this work, the syntheses, NLO properties,

* Corresponding author.
** Corresponding author.
E-mail addresses: qunjing@xju.edu.cn (Q. Jing), dhm@xju.edu.cn (H. Duan).

https://doi.org/10.1016/j.optmat.2023.114620
Received 12 October 2023; Received in revised form 17 November 2023; Accepted 19 November 2023
Available online 28 November 2023

infrared (IR) spectra, thermal properties and first-principles calculations of the title compounds were presented.

2. Experimental section

2.1. Reagents

Rb_2CO_3 (99.8 %), CsCl (99.9 %), ZnO (99 %), $ZnCl_2$ (99 %), RbCl (99.5 %), RbF (99.8 %), CsF (99 %), $NH_4H_2PO_4$ (99 %), LiF (99.9 %) were purchased from Aladdin Chemical Co. Ltd. and used as received.

2.2. Synthesis

$RbZnPO_4$ and $CsZnPO_4$ were synthesized by high temperature solid-state reaction. Rb_2CO_3, ZnO and $NH_4H_2PO_4$ were mixed in 1 : 2: 2 M ratios, and triturated fully with agate mortar. The mixtures were pre-heated up to 350 °C for 24 h to discharge H_2O, NH_3 and CO_2 in muffle furnace. Then the muffle furnace was heated to 660 °C, with several intermediate grindings and mixings. Finally, the polycrystalline samples of $RbZnPO_4$ were obtained at 660 °C successfully. The polycrystalline sample of $CsZnPO_4$ was also synthesized by similar way. Differently, CsCl, $ZnCl_2$ and $NH_4H_2PO_4$ were mixed in 2 : 3: 10 M ratios and the calcination temperature of $CsZnPO_4$ was 580 °C.

2.3. Single crystal growth

Crystals of $RbZnPO_4$ and $CsZnPO_4$ were synthesized via the high-temperature solution method. The reagents of RbCl (1.2035 g), $ZnCl_2$ (0.9634 g), RbF (0.4900 g) and $NH_4H_2PO_4$ (2.4156 g) for $RbZnPO_4$ were mixed, ground completely and packed into a platinum crucible. They were heated to 830 °C from room temperature and held at the temperature for 24 h to obtain a transparent and homogeneous melt. Then they were cooled slowly to 750 °C at a rate of 2 °C/h. After that, they were further cooled quickly to the room temperature at a rate of 20 °C/h. The crystal of $CsZnPO_4$ was also grown by the similar temperature procedure. Differently, the reagents of $CsZnPO_4$ were CsF (2.5190 g), ZnO (1.3579 g), $NH_4H_2PO_4$ (5.7570 g), LiF (3.2374 g) and RbCl (1.5120 g) respectively. After dropping to 750 °C, it was lowered to 680 °C at the rate of 3 °C/h, then the temperature was cooled to room temperature at a rate of 50 °C/h. Finally, some block, transparent crystals (Fig. S1) were acquired successfully for further single-crystal structural determination.

2.4. Powder X-ray diffraction

At room temperature, the powder X-ray diffraction (XRD) data of the title compounds were determined by, Bruker D8 Advance X-ray diffractometer with Cu-Kα radiation ($\lambda = 1.5418$ Å). The scanning step size was 0.02°/s per step. The angle range 2θ was 10–70°. As Fig. S2 shown, the experimental powder XRD patterns of the two compounds were conformed to the calculated ones.

2.5. Single-crystal X-ray diffraction

The transparent and well-shaped single crystals with sizes of 0.02 × 0.18 × 0.015 mm^3 for $RbZnPO_4$ and 0.11 × 0.10 × 0.10 mm^3 for $CsZnPO_4$ were chosen for single-crystal XRD measurement. All diffraction data were obtained on a Bruker Smart APEX II single crystal diffractometer furnished with a charge-coupled device (CCD). The Bruker Suite software package was used to implement the reduction of data. Collection and integration of diffraction data using the SAINT program [36]. Digital absorption correction was performed using the grain surface indexing method provided with the SADABS program [36]. The structures were settled by the direct approach and refined by the full-matrix least-square method fitting on F^2 using SHELXL-2018 system [37]. The atomic symmetry was checked by the PLATON routine until upgrade to a highly symmetric space group [38]. The detailed crystal structure data and refinement parameters were summarized in Table 1. Atomic coordinates equivalent isotropic displacement parameters, selected bond lengths and the anisotropic displacement parameters were all demonstrated in Tables S1–S6 in the supporting information.

2.6. Infrared and UV–Vis–NIR diffuse reflectance spectroscopy

The IR spectra of $RbZnPO_4$ and $CsZnPO_4$ were obtained by the BRUKER VERTEX 70 spectrometer ranging from 400 to 4000 cm^{-1} (25–2.5 μm). About 5 mg pure samples were mixed completely with 500 mg dried KBr and pressed into thin slices for the experiment. The UV–Vis–NIR diffuse-reflectance data of the title compounds were collected by Shimadzu UV-3600 spectrophotometer ranging from 190 to 2600 nm at room temperature.

2.7. Thermal analysis

Thermal gravimetric (TG) analysis and differential scanning calorimetry (DSC) were measured on the HITACHI STA 7300 thermal analyzer under nitrogen atmosphere. The samples were placed in Al_2O_3 crucible and heated from 30 to 1400 °C at a rate of 10 °C/min, and then cooled to 200 °C at a rate of 10 °C/min under an atmosphere of flowing argongas.

2.8. Second-harmonic generation measurements

The powder second-harmonic generation (SHG) responses of $RbZnPO_4$ and $CsZnPO_4$ were measured on Q-switched Nd: YAG laser at the wavelength of 1064 nm using the Kurtz-Perry method [39]. The samples of the two compounds were milled and sifted out different measure ranges: 28–82, 82–94, 94–116, 116–195, 195–205. And KDP

Table 1
Crystal data and structure refinement for $RbZnPO_4$ and $CsZnPO_4$.

Empirical formula	$RbZnPO_4$	$CsZnPO_4$
Formula weight	245.81	293.25
Temperature/K	273.15	293
Wavelength/Å	0.71073	0.71073
Crystal system	Monoclinic	Orthorhombic
Space group	$P2_1$ (No. 4)	$Imm2$ (No. 44)
a (Å)	8.8547(5)	5.4346(3)
b (Å)	5.4076(4)	9.0825(4)
c (Å)	8.9475(6)	9.0924(4)
β (deg)	90.167(2)	90.00
Volume (Å^3), Z	428.43(5), 4	448.80(4), 4
Calculated density (Mg/m^3)	3.811	4.340
Absorption coefficient (mm^{-1})	17.272	13.708
F(000)	456	528
Crystal size (mm^3)	0.02 × 0.018 × 0.015	0.11 × 0.10 × 0.10
Theta range for data collection (deg)	3.24 to 27.49	4.37 to 29.35
Limiting indices	$-11 \le h \le 10$, $-7 \le k \le 6$, $-11 \le l \le 11$	$-7 \le h \le 7$, $-12 \le k \le 11$, $-11 \le l \le 12$
Reflections collected/unique	6804/1960 [R (int) = 0.0378]	3464/669 [R (int) = 0.0508]
Completeness (%)	99.4	98.9
Data/restraints/parameters	1960/1/128	669/13/49
Goodness-of-fit on F_o^2	1.145	1.128
Final R indices [$F_o^2 > 2\sigma(F_o^2)$][a]	$R_1 = 0.0498$, wR_2 = 0.1146	$R_1 = 0.0499$, wR_2 = 0.1110
R indices (all data)[a]	$R_1 = 0.0574$, wR_2 = 0.1171	$R_1 = 0.0509$, wR_2 = 0.1116
Flack parameters	0.00	0.5(3)
Refinement method	Full-matrix least-squares on F^2	
Extinction coefficient	0.0156(12)	0.0036(12)
Largest diff. peak and hole (e·Å^{-3})	1.673 and −1.519	2.105 and −2.147

[a] $R_1 = \Sigma||F_o| - |F_c||/\Sigma|F_o|$ and $wR_2 = [\Sigma w(F_o^2 - F_c^2)^2/\Sigma wF_o^4]^{1/2}$ for $F_o^2 > 2\sigma(F_o^2)$.

samples with the same particle sizes were used as the references.

2.9. Theoretical calculations

The electronic structures and optical properties of $RbZnPO_4$ were calculated by CASTEP code [40]. During the calculation, the generalized gradient approximation of Perdew-Buker-Ernzerhof [41,42] was utilized. The valence electrons were set as Rb $4s^24p^65s^1$, Zn $3p^63d^{10}4s^2$, P $3s^23p^3$, and O $2s^22p^4$ under the norm-conserving pseudopotentials [43,44]. The kinetic energy cutoff of 680 eV was determined, and the numerical integration of the Brillouin zone was performed using $3 \times 5 \times 3$ Monkhorst-Pack k-point sampling [45]. The Heyd-Scuseria-Ernzerhof (HSE06) hybrid functional was carried out to provide a more accurate bandgap [46] using PWmat code. The refractive indices and the birefringence were further calculated via the OptaDOS code [47].

3. Results and discussion

3.1. Crystal structure

Although $RbZnPO_4$ and $CsZnPO_4$ crystallize in different space groups ($P2_1$ and *Imm*2, respectively), they both feature honeycomb-like topological structure consisting of corner-shared PO_4 and ZnO_4 tetrahedra. $RbZnPO_4$ crystallizes in the chiral space group $P2_1$ (No. 4) and the asymmetric units include $[Rb(1)O_{10}]/[Rb(2)O_9]$ polyhedra, $[ZnO_4]$ and $[PO_4]$ tetrahedron (Fig. 1 and Table S1). As depicted in Fig. 1a and b, the crystal structure of $RbZnPO_4$ can described as a 3D architecture structure, which consisting of $[Zn_2P_2O_{13}]_\infty$ layers in the *bc* plane and Rb atoms filling in the gap of the frame. From a topological perspective, the ZnO_4 and PO_4 groups can be seen as nodes and extend into a honeycomb-like skeleton (Fig. 1c). All the bond distances and angles are in the normal range, and the detailed atomic coordinate information are given in Tables S1 and S3. The calculated bond valence for $RbZnPO_4$ are summarized in Table S7.

$CsZnPO_4$ crystallizes in the orthorhombic crystal system with a polar asymmetric space group *Imm*2 (No. 44) and the asymmetric units comprises of $[Cs(1)O_{12}]/[Cs(2)O_{12}]$ polyhedron and $[(Zn|P)O_4]$ tetrahedra. One disordered oxygen splits into two positions of 0.5 each. (Fig. 2 and Table S2). As depicted in Fig. 2a and b, its structural framework is similar to $RbZnPO_4$ except replacing the $[Zn_2P_2O_{13}]_\infty$ in $RbZnPO_4$ to $[(Zn|P)_2O_7]_\infty$ in $CsZnPO_4$ and finally the Cs atoms fill the gaps of the frame. From a topological perspective, the ZnO_4 and PO_4 groups can be seen as nodes and extended into a honeycomb-like skeleton (Fig. 2c). All the bond distances and angles are in the normal range, and the detailed atomic coordinate information are given in Tables S2 and S4. The calculated bond valence for $CsZnPO_4$ are summarized in Table S8.

3.2. Thermal behavior analysis

TG-DSC curves of $RbZnPO_4$ and $CsZnPO_4$ are shown in Fig. S3. From the TG curves, there are no obvious weight loss up to 1250 °C for two compounds, which indicates they have good thermal stability. The weight losses of $RbZnPO_4$ and $CsZnPO_4$ start at 1251 °C and 1259 °C, which may be attributed to the decomposition of orthophosphates by releasing gaseous oxides containing P. There are two exothermic peaks (970 °C for $RbZnPO_4$ and 995 °C for $CsZnPO_4$) on the cooling curve, which maybe the phase change points. However, there was no obvious endothermic peak on the heating curve, indicating that the melting points of the two compounds should be higher than 1400 °C.

3.3. Spectroscopy analysis

IR spectra of $RbZnPO_4$ and $CsZnPO_4$ are plotted in Fig. S4, their IR spectra possess a certain degree of similarity. Peaks near 1130 and 1018 cm^{-1} for $RbZnPO_4$, 1140 and 1055 cm^{-1} for $CsZnPO_4$ are assigned to the asymmetric PO_4 stretching vibrations. The asymmetric PO_4 bending vibrations are revealed by the peaks near 574-466 cm^{-1} for $RbZnPO_4$ and 625-580 cm^{-1} for $CsZnPO_4$. IR spectra confirm the existence of PO_4 units, which are consistent with the results derived from the single crystal X-ray structural analyses and previous reported phosphates [7,48].

As presented in Fig. 3, the two crystals exhibit broad transmission, indicating that the application of $RbZnPO_4$ and $CsZnPO_4$ crystals can cover a spectral range from UV to near-infrared. Obviously, the UV absorption edges of the two compounds are about 226 and 231 nm. The absorption data are converted from the diffuse-reflectance data using the Kubelka-Munk function: $F(R)=K/S = (1-R)^2/2R$, where K is the absorption coefficient, S is the scattering coefficient, R is the reflectance [49], and the experimental band gaps of $RbZnPO_4$ and $CsZnPO_4$ are 5.49 and 5.37 eV, respectively.

3.4. Second-harmonic generation properties

As both $RbZnPO_4$ and $CsZnPO_4$ crystallize in NCS space groups, their SHG intensities are evaluated by means of the powder measurements. As illustrated in Fig. 4, $RbZnPO_4$ and $CsZnPO_4$ are type-I phase-matchable by Kurtz and Perry. The SHG intensities of $RbZnPO_4$ and $CsZnPO_4$ are ~1.2 and~0.5 × KDP, which are comparable with those of phosphates, such as $A_3Al_2(PO_4)_3$ (A = K, Rb) (0.4–0.6 × KDP) [50], $LiZnP_3O_9$ (0.2 × KDP) [51], $LiM_3P_2O_7$ (M = Na, K) (0.2–0.25 × KDP) [52]. To better understand the structure-property relationship, we made structure topological of the two compounds. As seen in the topological graph of $RbZnPO_4$ and $CsZnPO_4$ (Figs. 1c and 2c), the angle of the six-membered rings (6-MRs) range from 109.39° to 125.17° in $RbZnPO_4$, and from

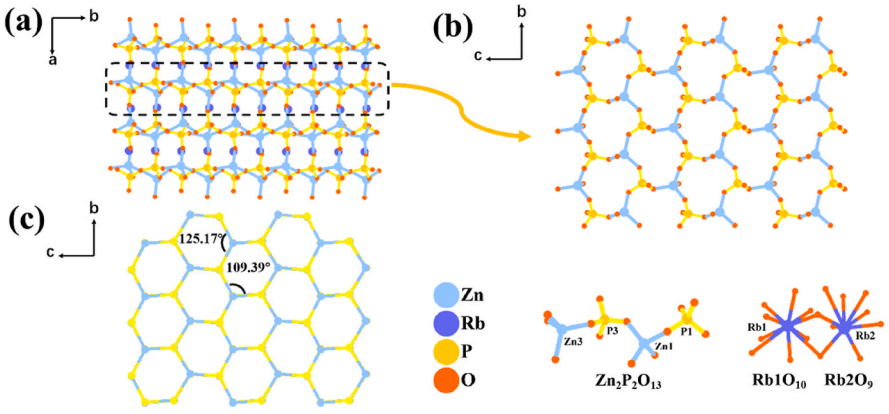

Fig. 1. Crystal structure features of $RbZnPO_4$. The $[Zn_2P_2O_{13}]_\infty$ layers stack along *c*-axis direction for $RbZnPO_4$ (a); and *a*-axis direction for $RbZnPO_4$ (b); Topological structure of a single layer. The blue and yellow spheres represent ZnO_4 and PO_4 groups, respectively (c).

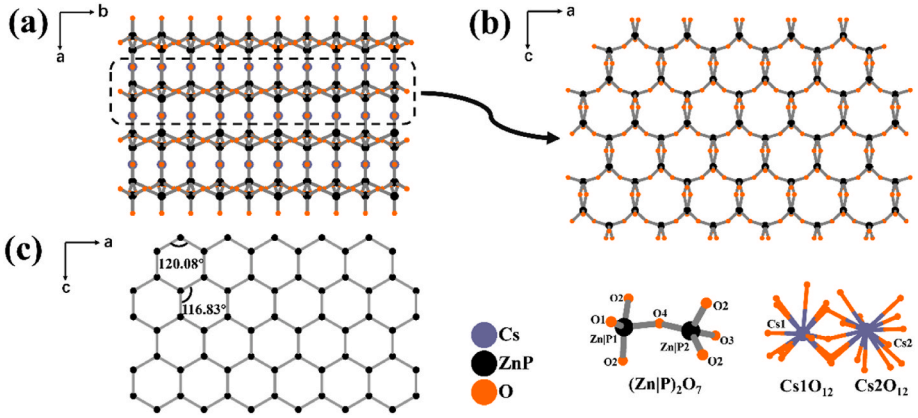

Fig. 2. Crystal structural features of $CsZnPO_4$. The $[(Zn|P)_2O_7]_\infty$ layers stack along *c*-axis direction for $CsZnPO_4$ (a); and *b*-axis direction for $CsZnPO_4$ (b); Topological structure of a single layer. The black spheres $(Zn|P)O_4$ (c).

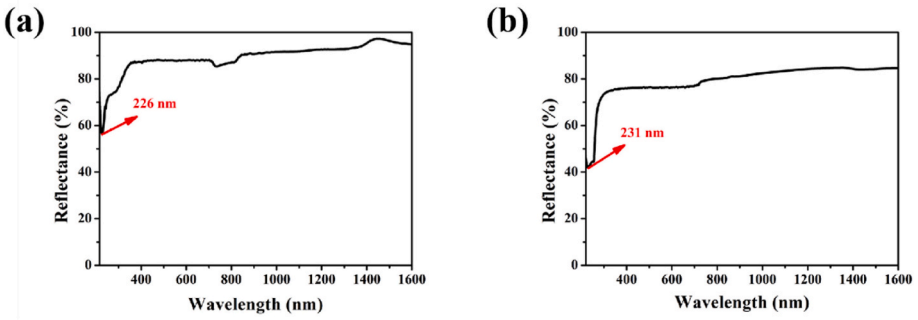

Fig. 3. UV–Vis–NIR diffuse reflectance spectra of $RbZnPO_4$ (a) and $CsZnPO_4$ (b).

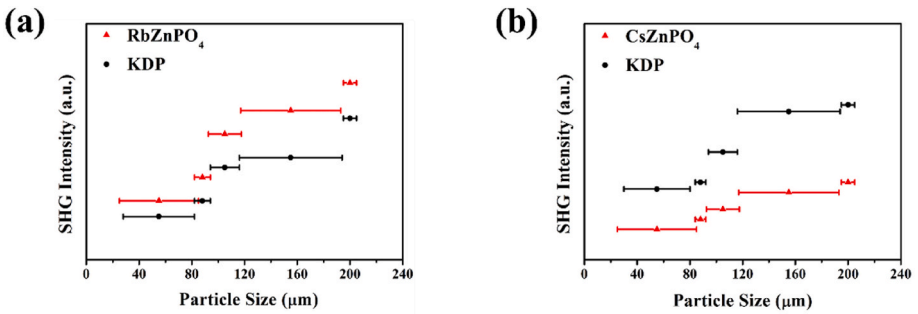

Fig. 4. The SHG intensity of $RbZnPO_4$ (a) and $CsZnPO_4$ (b) under laser radiation at 1064 nm. KDP serves as the reference.

116.83° to 120.08° in $CsZnPO_4$. In addition, the side lengths of the 6-MRs are in the range of 3.00–3.20 Å in $RbZnPO_4$ while 3.13–3.25 Å in $CsZnPO_4$. It is obvious that the topological 6-MRs of the $RbZnPO_4$ is significantly more deformable than the $CsZnPO_4$, which should be the structural reason for their different SHG responses. $RbZnPO_4$ has a good NLO structure compared with $CsZnPO_4$.

3.5. Computational details descriptions

Owing to the disorder structure, $CsZnPO_4$ was not included in the calculation (Table S9). As the NLO properties are highly dependent on the features of the valence and conduction band edges, the band structures and the densities of states have been systematically studied. $RbZnPO_4$ is direct band gap compound at G point and its theoretical band gap is 5.43 eV (absorption edges corresponding to 228 nm) by HSE06 functional (Fig. 5). The more detailed analysis of the top of the valence band (VB) and the bottom of the conduction band (CB) are carried out. The calculated partial density of states (PDOS) is shown in Fig. 6. The top of VB near the Fermi level from −4 to 0 eV is composed of the O 2p, P 3s, 3p and Zn 3d orbitals. The bottom of CB near the Fermi level from 0 to 4 eV is composed of P 3s, 3p and Zn 4s, 3p orbitals. These indicate that the Zn–O and P–O units should give the mainly contribution to the optical properties. In addition, the SHG coefficient d_{ij} was calculated. $RbZnPO_4$ has four nonzero independent SHG coefficients ($d_{14} = -0.424$ p.m./V, $d_{16} = -0.427$ p.m./V, $d_{22} = 1.374$ p.m./V, and $d_{23} = -1.420$ p.m./V), the obtained effective SHG response is $d_{eff} = 0.5367$ pm/V (~1.38 × KDP), and is close to the experimentally measured value. To investigate the contribution of each atom for SHG response, we performed the SHG density calculation of $RbZnPO_4$ (Fig. S5), the SHG process can be described by two virtual transition processes, virtual electron (VE) and virtual hole (VH) processes. We only show the SHG density of VE process because it has major contribution to SHG. It is clearly to see the main contribution coming from O-2p, P-3s, P-3p orbitals in VE processes. As shown in Fig. S6, the calculated refractive

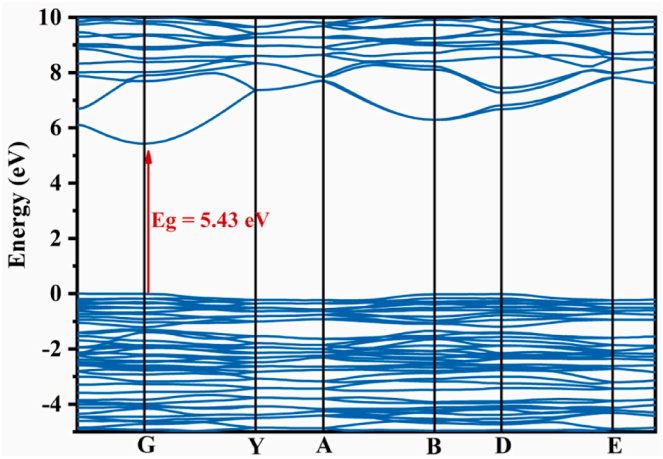

Fig. 5. Band structures of $RbZnPO_4$ by HSE06 hybrid functional.

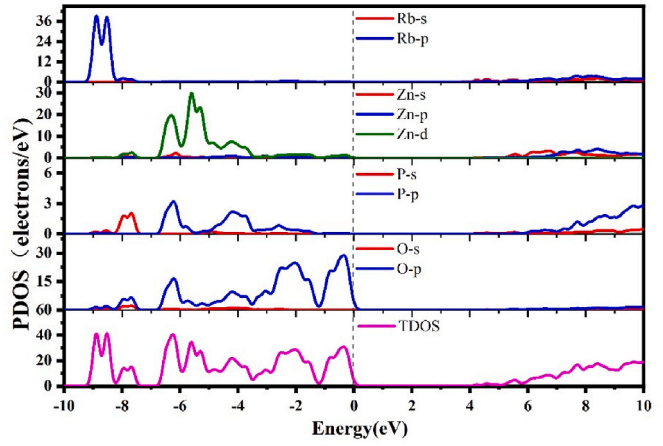

Fig. 6. Partial density of states of $RbZnPO_4$.

index curve indicates that n_x-n_y < n_y-n_z in the wavelength range of 300–1800 nm, making it a negative biaxial crystal. The birefringence ($\Delta n = n_x$-n_y) is 0.0078 at 1064 nm. The authors believe the first-principles method underestimated the birefringence because the relatively small birefringence is uneasy to meet the phase matching condition, but the phase matching condition was observed in Fig. 4. More accurate but more expensive method like TDDFT would be adopted to get more reliable refractive indices and birefringence values. It is well known that introduction of F, N, or $[OH]^-$ et al. can greatly enhance birefringence, so we would try to introduce these elements to increase the birefringence like Pan, Xie and Ok do in reference [4,53,54].

4. Conclusion

In summary, we obtained two NLO materials $RbZnPO_4$ and $CsZnPO_4$, they crystallize in different space groups. We studied their structural features and performances in terms of experimental measurement and first-principles calculations. Remarkably, both compounds exhibit mild powder SHG responses (1.2 and 0.5 × KDP for $RbZnPO_4$ and $CsZnPO_4$) with type I phase matching behaviors and short absorption edges (226 nm for $RbZnPO_4$ and 231 nm for $CsZnPO_4$). These works will enlighten subsequent studies on designing novel inorganic phosphates with different structures and functional properties.

CRediT authorship contribution statement

Qun Jing: Writing – original draft, Funding acquisition, Conceptualization, Data curation. **Menglin Zhu:** Formal analysis, Investigation. **Lu Li:** Software. **Xu Ji:** Software. **Haiming Duan:** Writing – review & editing. **Henglei Chen:** Writing – review & editing, Funding acquisition. **Ming-Hsien Lee:** Writing – review & editing.

Declaration of competing interest

The authors declare no conflict of interest to this work.

Data availability

Data will be made available on request.

Acknowledgment

This work has been supported by the National Natural Science Foundation of China (Grant No. 12264047), the Natural Science Foundation of Xinjiang Uygur Autonomous Region of China (2022D01C51), and the Tianshan Talent Project of Xinjiang Uygur Autonomous Region of China (2022TSYCJU0004).

Appendix A. Supplementary data

Supplementary data to this article can be found online at https://doi.org/10.1016/j.optmat.2023.114620.

References

[1] D.F. Eaton, Nonlinear optical materials, Science 253 (1991) 281–287, https://doi.org/10.1126/science.253.5017.281.
[2] P.S. Halasyamani, K.R. Poeppelmeier, Noncentrosymmetric oxides, Chem. Mater. 10 (1998) 2753–2769, https://doi.org/10.1021/cm980140w.
[3] M. Mutailipu, J. Han, Z. Li, F. Li, J. Li, F. Zhang, X. F Long, Z. Yang, S. Pan, Achieving the full-wavelength phase-matching for efficient nonlinear optical frequency conversion in $C(NH_2)_3BF_4$, Nat. Photonics 17 (2023) 694–701, https://doi.org/10.1038/s41566-023-01228-7.
[4] Y. Li, J. Lee, K.M. Ok, $KHC_2O_4{\cdot}B(OH)_3$: a nonlinear optical crystal with large birefringence in the short-wavelength ultraviolet region, Bull. Kor. Chem. Soc. 44 (2023) 788–793, https://doi.org/10.1002/bkcs.12720.
[5] P. Yu, L. Wu, L. Zhou, L. Chen, Deep-ultraviolet nonlinear optical crystals: $Ba_3P_3O_{10}X$ (X = Cl, Br), J. Am. Chem. Soc. 136 (2013) 480–487, https://doi.org/10.1021/ja411272y.
[6] L. Li, Y. Wang, B. Lei, S. Han, Z. Yang, K.R. Poeppelmeier, S. Pan, A new deep-ultraviolet transparent orthophosphate $LiCs_2PO_4$ with large second harmonic generation response, J. Am. Chem. Soc. 138 (2016) 9101–9104, https://doi.org/10.1021/jacs.6b06053.
[7] B. Wu, C. Hu, F. Mao, R. Tang, J. Mao, Highly polarizable Hg^{2+} induced a strong second harmonic generation signal and large birefringence in $LiHgPO_4$, J. Am. Chem. Soc. 141 (2019) 10188–10192, https://doi.org/10.1021/jacs.9b05125.
[8] J. Chen, L. Xiong, L. Chen, L. Wu, $Ba_2NaClP_2O_7$: unprecedented phase matchability induced by symmetry breaking and its unique fresnoite-type structure, J. Am. Chem. Soc. 140 (2018) 14082–14086, https://doi.org/10.1021/jacs.8b10209.
[9] J. Lv, Y. Qian, Q. Jing, X. Wang, M.H. Lee, Z. Chen, Two metal phosphate nonlinear optical materials simultaneously exhibiting ultraviolet transparence and a large birefringence, Chem. Mater. 34 (2022) 5919–5927, https://doi.org/10.1021/acs.chemmater.2c00825.
[10] B. Zhang, G. Han, Y. Wang, X. Chen, Z. Yang, S. Pan, Expanding frontiers of ultraviolet nonlinear optical materials with fluorophosphates, Chem. Mater. 30 (2018) 5397–5403, https://doi.org/10.1021/acs.chemmater.8b02223.
[11] Y. Sun, G. Liu, Y. Lv, L. Ma, W. Yao, R. Tang, $(NH_4)_3(H_3O)Zn_4(PO_4)_4$: a nonlinear optical zinc orthophosphate crystal, J. Solid State Chem. 325 (2023), 124171, https://doi.org/10.1016/j.jssc.2023.124171.
[12] X. Chen, Q. Jing, K.M. Ok, $Pb_{18}O_8Cl_{15}I_5$: a polar lead mixed oxyhalide with unprecedented architecture and excellent infrared nonlinear optical properties, Angew. Chem. Int. Ed. 59 (2020) 20323–20327, https://doi.org/10.1002/anie.202009541.
[13] T. Yu, L. Xiong, X. Liu, Y. Yang, Z. Lin, L. Wu, L. Chen, $AZn(PO_3)_3$ (A = K, Rb): deep-ultraviolet nonlinear optical phosphates derived from synergy of a unique $[ZnO_6]$ octahedron and a $[PO_3]_\infty$ chain, Cryst. Growth Des. 21 (2021) 2445–2452, https://doi.org/10.1021/acs.cgd.1c00051.
[14] M. Mutailipu, F. Li, C. Jin, Z. Yang, K.R. Poeppelmeier, S. Pan, Strong nonlinearity induced by coaxial alignment of polar chain and dense $[BO_3]$ units in $CaZn_2(BO_3)_2$, Angew. Chem., Int. Ed. 61 (2022), e202202096, https://doi.org/10.1002/anie.202202096.
[15] H. Yu, W. Zhang, J. Young, J.M. Rondinelli, P.S. Halasyamani, Design and synthesis of the beryllium-free deep-ultraviolet nonlinear optical material

$Ba_3(ZnB_5O_{10})PO_4$, Adv. Mater. 27 (2015) 7380–7385, https://doi.org/10.1002/adma.201503951.
[16] H. Yu, H. Wu, S. Pan, Z. Yang, X. Hou, X. Su, Q. Jing, K.R. Poeppelmeier, J. M. Rondinelli, $Cs_3Zn_6B_9O_{21}$: a chemically benign member of the KBBF family exhibiting the largest second harmonic generation response, J. Solid State Chem. 136 (2014) 1264–1267, https://doi.org/10.1021/ja4117389.
[17] Y. Chen, M. Zhang, M. Mutailipu, K. Poeppelmeier, S. Pan, Research and development of zincoborates: crystal growth, structural chemistry and physicochemical properties, Molecules 24 (2019) 2763, https://doi.org/10.3390/molecules24152763.
[18] G. Zou, K.M. Ok, Novel ultraviolet (UV) nonlinear optical (NLO) materials discovered by chemical substitution-oriented design, Chem. Sci. 11 (2020) 5404–5409, https://doi.org/10.1039/d0sc01936d.
[19] G. Peng, N. Ye, Z. Lin, L. Kang, S. Pan, M. Zhang, C. Lin, X. Long, M. Luo, Y. Chen, Y. Tang, F. Xu, T. Yan, NH4Be2BO3F2 and γ-Be2BO3F: overcoming the layering habit in $KBe_2BO_3F_2$ for the next-generation deep-ultraviolet nonlinear optical materials, Angew. Chem., Int. Ed. 130 (2018) 9106–9110, https://doi.org/10.1002/ange.201803721.
[20] L. Mei, Y. Wang, C. Chen, B. Wu, Nonlinear optical materials based on $MBe_2BO_3F_2$ (M = Na, K), J. Appl. Phys. 74 (1993) 7014–7015, https://doi.org/10.1063/1.355060.
[21] C. Chen, S. Luo, X. Wang, G. Wang, X. Wen, H. Wu, X. Zhang, Z. Xu, Deep uv nonlinear optical crystal: $RbBe_2(BO_3)F_2$, J. Opt. Soc. Am. B 26 (2009) 1519–1525, https://doi.org/10.1364/josab.26.001519.
[22] H. Huang, C. Chen, X. Wang, Y. Zhu, G. Wang, X. Zhang, L. Wang, J. Yao, Ultraviolet nonlinear optical crystal: $CsBe_2BO_3F_2$, J. Opt. Soc. Am. B 28 (2011) 2186–2190, https://doi.org/10.1364/josab.28.002186.
[23] G. Shi, Y. Wang, F. Zhang, B. Zhang, Z. Yang, X. Hou, S. Pan, K.R. Poeppelmeier, Finding the next deep-ultraviolet nonlinear optical material: $NH_4B_4O_6F$, J. Am. Chem. Soc. 139 (2017) 10645–10648, https://doi.org/10.1021/jacs.7b05943.
[24] Z. Zhang, Y. Wang, B. Zhang, Z. Yang, S. Pan, Polar Fluorooxoborate, NaB_4O_6F: a promising material for ionic conduction and nonlinear optics, Angew. Chem., Int. Ed. 57 (2018) 6577–6581, https://doi.org/10.1002/anie.201803392.
[25] F. Liang, L. Kang, P. Gong, Z. Lin, Y. Wu, Rational design of deep-ultraviolet nonlinear optical materials in fluorooxoborates: toward optimal planar configuration, Chem. Mater. 29 (2017) 7098–7102, https://doi.org/10.1021/acs.chemmater.7b03162.
[26] Y. Wang, B. Zhang, Z. Yang, S. Pan, Cation-tuned synthesis of fluorooxoborates: towards optimal deep-ultraviolet nonlinear optical materials, Angew. Chem., Int. Ed. 130 (2018) 2172–2176, https://doi.org/10.1002/ange.201712168.
[27] X. Wang, Y. Wang, B. Zhang, F. Zhang, Z. Yang, S. Pan, CsB_4O_6F: a congruent-melting deep-ultraviolet nonlinear optical material by combining superior functional units, Angew. Chem., Int. Ed. 129 (2017) 14307–14311, https://doi.org/10.1002/ange.201708231.
[28] G. Zou, N. Ye, L. Huang, X. Lin, Alkaline-alkaline earth fluoride carbonate crystals $ABCO_3F$ (A = K, Rb, Cs; B = Ca, Sr, Ba) as nonlinear optical materials, J. Am. Chem. Soc. 133 (2011) 20001–20007, https://doi.org/10.1021/ja209276a.
[29] Q. Li, G. Zou, C. Lin, N. Ye, Synthesis and characterization of $CsSrCO_3F$-a beryllium-free new deep-ultraviolet nonlinear optical material, New J. Chem. 40 (2016) 2243–2248, https://doi.org/10.1039/c5nj03059e.
[30] H. Yu, J. Young, H. Wu, W. Zhang, J.M. Rondinelli, P.S. Halasyamani, $M_4Mg_4(P_2O_7)_3$ (M = K, Rb): structural engineering of pyrophosphates for nonlinear optical applications, Chem. Mater. 29 (2017) 1845–1855, https://doi.org/10.1021/acs.chemmater.7b00167.
[31] X. Lu, Z. Chen, X. Shi, Q. Jing, M.H. Lee, Two pyrophosphates with large birefringences and second-harmonic responses as ultraviolet nonlinear optical materials, Angew. Chem., Int. Ed. 132 (2020) 17801–17809, https://doi.org/10.1002/ange.202007494.
[32] L. Qi, Z. Chen, X. Shi, X. Zhang, Q. Jing, N. Li, Z. Jiang, B. Zhang, M.-H. Lee, $A_3BBi(P_2O_7)_2$(A = Rb, Cs; B = Pb, Ba): isovalent cation substitution to sustain large second-harmonic generation responses, Chem. Mater. 32 (2020) 8713–8723, https://doi.org/10.1021/acs.chemmater.0c03383.
[33] S. Liu, B. Zhang, H. Wu, H. Yu, Z. Hu, J. Wang, Y. Wu, Ultraviolet nonlinear optical crystals $A_3SrBi(P_2O_7)_2$(A = K, Rb) with large second harmonic generation responses, Inorg. Chem. Front. 8 (2021) 2061–2067, https://doi.org/10.1039/d0qi01445a.
[34] X. He, L. Qi, W. Zhang, R. Zhang, X. Dong, J. Ma, M. Abudoureheman, Q. Jing, Z. Chen, Controlling the nonlinear optical behavior and structural transformation with a-site cation in α-$AZnPO_4$(A = Li, K), Small 19 (2023), 2206991, https://doi.org/10.1002/smll.202206991.
[35] L. Elammari, B. Elouadi, Structure cristalline de $RbZnPO_4$, J. Chim. Phys. 88 (1991) 1969–1974, https://doi.org/10.1051/jcp/1991881969.
[36] V. Saint, 7.60 A, Bruker Analytical X-Ray Instruments, Inc., Madison, WI, 2008.
[37] G.M. Sheldrick, Crystal structure refinement with SHELXL, Acta Crystallogr. C 71 (2015) 3–8, https://doi.org/10.1107/s2053229614024218.
[38] A.L. Spek, Single-crystal structure validation with the program PLATON, J. Appl. Crystallogr. 36 (2003) 7–13, https://doi.org/10.1107/s0021889802022112.
[39] S.K. Kurtz, T.T. Perry, A powder technique for the evaluation of nonlinear optical materials, J. Appl. Phys. 39 (1968) 3798–3813, https://doi.org/10.1063/1.1656857.
[40] S.J. Clark, M.D. Segall, C.J. Pickard, P.J. Hasnip, M.I.J. Probert, K. Refson, M. C. Payne, First principles methods using CASTEP, Z. für Kristallogr. - Cryst. Mater. 220 (2005) 567–570, https://doi.org/10.1524/zkri.220.5.567.65075.
[41] D.M. Ceperley, B.J. Alder, Ground state of the electron gas by a stochastic method, Phys. Rev. Lett. 45 (1980) 566–569, https://doi.org/10.1103/PhysRevLett.45.566.
[42] J.P. Perdew, K. Burke, M. Ernzerhof, Generalized gradient approximation made simple, Phys. Rev. Lett. 77 (1996) 3865–3868, https://doi.org/10.1103/PhysRevLett.77.3865.
[43] D.R. Hamann, M. Schlüter, C. Chiang, Norm-Conserving pseudopotentials, Phys. Rev. Lett. 43 (1979) 1494–1497, https://doi.org/10.1103/PhysRevLett.43.1494.
[44] L. Kleinman, D.M. Bylander, Efficacious form for model pseudopotentials, Phys. Rev. Lett. 48 (1982) 1425–1428, https://doi.org/10.1103/PhysRevLett.48.1425.
[45] H.J. Monkhorst, J.D. Pack, Special points for brillouin-zone integrations, Phys. Rev. B 13 (1976) 5188–5192, https://doi.org/10.1103/PhysRevB.13.5188.
[46] M.K.Y. Chan, G. Ceder, Efficient band gap prediction for solids, Phys. Rev. Lett. 105 (2010), 196403, https://doi.org/10.1103/PhysRevLett.105.196403.
[47] A.J. Morris, R.J. Nicholls, C.J. Pickard, J.R. Yates, Optados: a tool for obtaining density of states, core-level and optical spectra from electronic structure codes, Comput, Phys. Commun. 185 (2014) 1477–1485, https://doi.org/10.1016/j.cpc.2014.02.013.
[48] Z. Chen, Y. Fang, W. Zhang, W. Chen, X. Lu, Q. Jing, M.H. Lee, $ALiZnP_2O_7$ (A = Rb, Cs): two mixed alkali zinc pyrophosphates featuring a $[Li_2Zn_2P_4O_{20}]^{14-}$ anionic skeleton, Inorg. Chem. 57 (2018) 10568–10575, https://doi.org/10.1021/acs.inorgchem.8b01140.
[49] J. Tauc, Absorption edge and internal electric fields in amorphous semiconductors, Mater. Res. Bull. 5 (1970) 721–729, https://doi.org/10.1016/0025-5408(70)90112-1.
[50] M. Wen, H. Wu, S. Cheng, J. Sun, Z. Yang, X. Wu, S. Pan, Experimental characterization and first principles calculations of linear and nonlinear optical properties of two orthophosphates $A_3Al_2(PO_4)_3$(A = Rb, K), Inorg. Chem. Front. 6 (2019) 504–510, https://doi.org/10.1039/c8qi01249k.
[51] Z. Xie, X. Su, H. Ding, H. Li, Crystal structures and theoretical studies of polyphosphate $LiZnP_3O_9$ for nonlinear optical applications, J. Solid State Chem. 262 (2018) 313–319, https://doi.org/10.1016/j.jssc.2018.03.032.
[52] Y. Shi, Y. Wang, S. Pan, Z. Yang, X. Dong, H. Wu, M. Zhang, J. Cao, Z. Zhou, Synthesis, crystal structures and optical properties of two congruent-melting isotypic diphosphates: $LiM_3P_2O_7$(M = Na, K), J. Solid State Chem. 197 (2013) 128–133, https://doi.org/10.1016/j.jssc.2012.08.038.
[53] W. Jin, C. Xie, X. Hou, M. Cheng, E. Tikhonov, M. Wu, S. Pan, Z. Yang, From monofluorophosphates A_2PO_3F to difluorophosphates APO_2F_2 (A = alkali metal): design of a potential deep-ultraviolet nonlinear optical materials system with a shortened phase-matching wavelength, Chem. Mater. 35 (2023) 5281–5290, https://doi.org/10.1021/acs.chemmater.3c00291.
[54] C. Xie, A. Tudi, A.R. Oganov, PNO: a promising deep-UV nonlinear optical material with the largest second harmonic generation effect, Chem. Commun 58 (2022) 12491–12494, https://doi.org/10.1039/d2cc02364d.